

Analysis of phase shift between oscillations of pressure and flame radiation intensity of self-excited combustion instabilities

S. Gröning^{*†} and J. S. Hardi^{*} and D. Suslov^{*} and M. Oswald^{*.**}

^{*}German Aerospace Center (DLR), Institute of Space Propulsion
Im Langen Grund, 74239 Hardthausen, Germany

^{**}Institute of Jet Propulsion and Turbomachinery, RWTH Aachen University
Templergraben 55, 52062 Aachen, Germany

[†]Corresponding author

Abstract

The energy transfer from the heat release of the combustion to the acoustic pressure oscillations is the driving element of combustion instabilities. This energy transfer is described by the Rayleigh criterion and depends on the phase shift between the pressure and heat release rate oscillations. A research rocket combustor operated with the propellant combination hydrogen/oxygen was equipped with dynamic pressure sensors and fibre optical probes to measure the flame radiation. This setup has been used for a phase shift analysis study which showed that unstable operation is characterised by a phase shift leading to an energy transfer from the heat release to the acoustic pressure oscillations.

1. Introduction

High frequency combustion instability in liquid propellant rocket engines (LPREs) is a problem which is known since the beginning of the development of these engines.¹ Extensive studies have been carried out all over the world starting in the 1950's.²⁻⁴ Due to the complexity of the problem reliable predictive capabilities could not be developed so far. Experimental research of combustion instabilities aims at understanding the underlying physical processes and mechanisms being responsible for this phenomenon. This fundamental knowledge is required for the development of stability prediction tools.^{5,6}

The random pressure oscillations created by the combustion process or by turbulence cause an excitation of the acoustic resonance modes of the combustion chamber. These oscillations can result in oscillatory combustion causing a periodic modulation of the heat release rate. Rayleigh postulated in 1878 that an acoustic oscillation is excited if heat is added at the moment of greatest compression or subtracted at the moment of greatest expansion.^{7,8} This so called Rayleigh criterion has been formulated in a simple mathematical way by Putnam and Dennis.^{9,10}

$$\int_{\text{cycle}} \dot{q}' p' dt > 0 \quad (1)$$

This formulation neglects damping and requires that the time integral over a cycle of the oscillation of the pressure p' and the volumetric heat release rate \dot{q}' must be greater than zero. If mono frequent oscillations are assumed this means that the absolute value of the phase angle between both oscillations must be between 0 and $\pi/2$. If the Rayleigh criterion is fulfilled energy is transferred from the heat release to the acoustic oscillations. This causes a rapid increase of the acoustic pressure oscillation amplitudes which can lead to damage or even the destruction of the whole engine, which is then called combustion instability.¹¹ If the absolute values of the phase angle is between $\pi/2$ and π the oscillation is damped.

Self-excited combustion instabilities of the first tangential (1T) mode were found in a research hydrogen/oxygen rocket engine combustor named BKD. During unstable operation the amplitude of the pressure oscillation shows large fluctuations.¹² This is an indication that the Rayleigh criterion according to eq. (1) is not permanently fulfilled causing a varying energy transfer. The research combustor BKD is equipped with dynamic pressure sensors to measure the acoustic pressure oscillations and fibre optical probes to analyse the oscillation of the combustion process. This setup

can be used as an experimental platform in order to analyse the pressure and heat release rate oscillation according to eq. (1). In the past phase shift analysis studies were performed especially under forced excitation conditions.¹³⁻¹⁷ But also self-excited combustion instabilities in a laboratory-scale combustor have been analysed under this research question.¹⁸ The BKD offers an experimental platform to extend this analysis to self-excited combustion instabilities under representative conditions for LPREs with the cryogenic propellant combination hydrogen/oxygen. In this work, a first phase shift analysis study is presented in order to evaluate a newly developed methodology to analyse the data of the BKD test runs with regard to the phase shift between pressure and flame radiation intensity oscillation.

A pressure field reconstruction procedure¹⁹ is used to process the dynamic pressure sensor signals and calculate the amplitude and orientation of the 1T mode pressure field. With the aforementioned fibre optical probes the OH* flame emission is measured for selected positions. The results of the pressure field reconstruction procedure are used to calculate the pressure oscillation for the selected positions observed by the fibre optical probes. As a result for each position two signals are obtained which are used for a phase shift analysis study.

Using this methodology two selected load points, one stable and one unstable have been analysed. In both cases the phase shift is continuously varying and shows a fluctuating behaviour on the time scales of the 1T oscillation period. Statistical analysis were performed on the obtained phase shift signals in order to identify any structure. For both load points on large time scales all phase shift signals show a rather continuous increase or decrease showing that the pressure and OH* intensity do not oscillate with the same frequency. A histogram analysis shows that the phase shift signals for the unstable load point are characterised by a concentration of samples in the region around a phase shift of zero which is in agreement with the Rayleigh criterion. The same analysis for the stable load point shows a different result. Here only a slight, much less pronounced concentration of samples can be found. This shows significantly different structures in the phase shift signals of a stable and unstable load point.

2. Experimental Setup

The test specimen used for this investigation is the research combustor BKD^{20,21} with the injector head L42 operated at the P8 test facility²²⁻²⁴ of the DLR Institute of Space Propulsion in Lampoldshausen. It consists of the injector head, the cylinder segment, and the nozzle segment as shown in Figure 1 on the left side. The L42 injector head has 42 shear coaxial injectors and is operated with the propellant combination hydrogen/oxygen. The combustion chamber has a cylindrical shape with a diameter of 80 mm. The nozzle throat diameter is 50 mm which leads to a contraction ratio of 2.56. The maximum combustion chamber pressure (p_{cc}) during the test run which was used for the presented analysis was 80 bar. The highest mixture ratio ($ROF = \dot{m}_{O_2}/\dot{m}_{H_2}$) was 6.0. For the load point $p_{cc} = 80$ bar with $ROF = 6.0$ the total propellant mass flow rate is 6.7 kg/s.

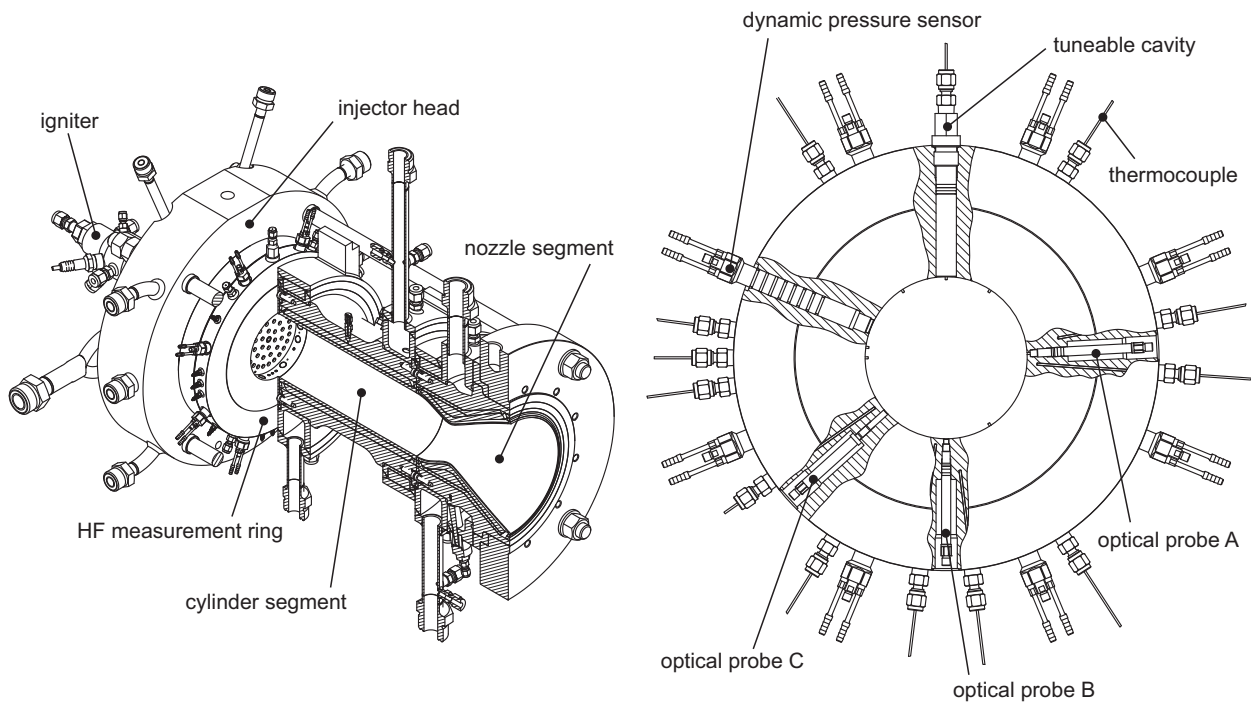


Figure 1: Combustion chamber BKD (left) with HF measurement ring (right)

According to eq. (1) the evaluation of the Rayleigh criterion requires the simultaneous measurement of the acoustic pressure oscillation $p'(t)$ and the volumetric heat release rate $\dot{q}'(t)$. The measurement of $p'(t)$ can be achieved relatively easy by the installation of dynamic pressure sensors. The measurement of $\dot{q}'(t)$ is much more challenging especially at the conditions found in rocket engines.²⁵ Usually the measurement of $\dot{q}'(t)$ is approximated using the flame radiation which is easy to measure. In hydrogen/oxygen combustion the radiation of the excited hydroxyl radical (OH*) has been used as a marker for $\dot{q}'(t)$ due to its good detectability.^{25,26}

In order to measure the $p'(t)$ oscillations in the combustion chamber as well as the fluctuations of the OH* intensity the BKD combustor has been equipped with a specially designed HF measurement ring as shown in Figure 1 on the right side. This ring is installed between the injector head and the cylindrical combustion chamber segment as shown in Figure 1 on the left side. It is equipped with 8 flush mounted water cooled Kistler dynamic pressure sensors with an equiangular spacing of 45°. The dynamic pressure sensor signals $p'_{\text{pdyn}}(t)$ are sampled with a sampling frequency of 100 kHz.

In order to measure the flame radiation at specific locations the HF measurement ring is equipped with 3 fibre optical probes. This method of obtaining an optical access to the combustion chamber with minor modifications of the engine is well known in the field of reciprocating engines.^{27,28} Due to higher seal demands when using hydrogen as a fuel this technology had to be adapted to LPREs with the propellant combination hydrogen/oxygen. A small sapphire rod is installed in the optical probe which creates the optical access. The full acceptance angle of the optical probes is approximately 2°. The radiation captured by the probes is transferred to photomultiplier (PM) detectors using an optical fibre. The PMs are equipped with interference filters with a centre wavelength of 310 nm. As discussed in detail in other work by the authors,²⁹ the OH* intensity signals measured by the PMs can be seen as an approximation for the oscillation of the \dot{q}' as they measure an integrated line of sight signal.²⁶ But it must be kept in mind, that the $\dot{q}'(t)$ signals are not identical to the PM signals. A variation of \dot{q}' is not the only cause for a variation of the OH* intensity. Nevertheless the PM signals are a measure for the flame dynamics at the injector exit. The phase shift analysis has therefore been performed between the $p'(t)$ signals and the OH* intensity signals $I'(t)$. Like the $p'_{\text{pdyn}}(t)$ signals also the $I'(t)$ signals are sampled with a sampling frequency of 100 kHz.

The narrow field of view of the fibre optical probes has been used to align the probes to 3 specific injectors of the outer ring of the injector pattern as shown in Figure 2. The selection of the injectors was based on the mode symmetry of the 1T mode. The angular distance between the nodal line and a pressure anti node of the 1T mode is 90°. Probe A and B were therefore aligned to the injectors 19 and 13 with an angular distance of 90°. Probe C was aligned to injector 10 with an angular distance of 45° to injector 13. Probe B was aligned to the centre of the injector while probes A and C were aligned tangentially to the reaction zone. The alignment of probes A and C has shown to improve the signal quality as a larger part of the reaction zone lies within the field of view. On the other hand this alignment is more sensitive to capture radiation coming from other injectors.

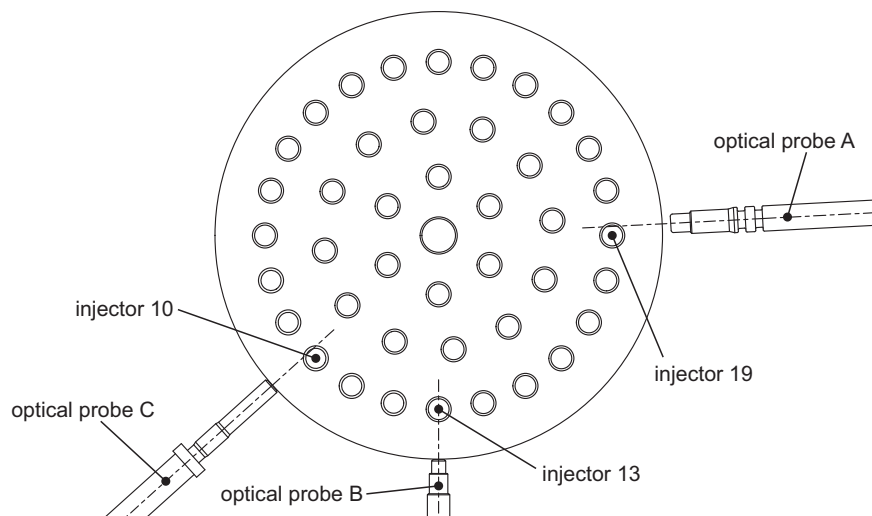


Figure 2: Alignment of fibre optical probes to selected injectors

3. Data Analysis Methodology

3.1 Pressure Field Reconstruction

The 1T mode pressure field reconstruction algorithm¹⁹ was originally developed for the CRC research combustor.³⁰ The pressure oscillations are measured on the wall of a cylindrical combustion chamber. The amplitude and orientation of the 1T pressure field as functions of time are determined in the measurement plane described by the dynamic pressure sensors. The procedure has been successfully applied to data from the BKD test series.^{12,21}

The basis of the pressure field reconstruction algorithm is the fact that the wall pressure distribution of the 1T mode is a sine function with one period in circumferential direction. The first step is to band pass filter the dynamic pressure sensor signals $p'_{\text{pdy}}(t)$ signals to extract only the contribution of the 1T mode. A two way filtering procedure³¹ in combination with a Butterworth filter of second order is used to avoid a phase shift of the signal during the band pass filtering. In the case of the BKD HF measurement ring for each time step of the $p'_{\text{pdy}}(t)$ signals 8 data points consisting of an angular position θ and a pressure value p' are available. A sine function with 3 parameters (A , φ_{pfr} , p_{off}) is fitted to this data set.

$$p'(\theta) = A \sin(\theta - \varphi_{\text{pfr}}) + p_{\text{off}} \quad (2)$$

If this sine function is known the whole 1T pressure field is known. This is done for every time step of the $p'_{\text{pdy}}(t)$ signals so as a result three signals $A(t)$, $\varphi_{\text{pfr}}(t)$, and $p_{\text{off}}(t)$ are obtained.

These 3 signals completely describe the temporal evolution of the 1T mode pressure field in the measurement plane of the HF measurement ring. They provide the possibility to calculate the $p'(t)$ signal of the 1T mode at any given position in this plane. Here they are used to calculate the $p'(t)$ signal of the 1T mode at the positions of the 3 injectors which were observed by the fibre optical probes.

3.2 Pressure Signal Calculation

Based on the fundamental equations of cylinder acoustics³² the pressure field of the 1T mode is described by

$$p'(r, \theta, t) = J_1\left(\frac{\pi\alpha_{01}r}{R}\right) [M \cos(\theta + \omega t - \delta_1) + N \cos(\theta - \omega t - \delta_2)] \quad (3)$$

where r and θ are the polar coordinates, t the time, J_1 the Bessel function of first order, α_{01} a root of the Bessel function depending on the resonance mode,³² R the radius of the cylinder, M and N amplitude constants, ω the oscillation frequency of the 1T mode and δ_1 and δ_2 phase constants. In order to obtain the wall pressure distribution eq. (3) must be evaluated on the cylinder wall ($r = R$).

$$p'(\theta, t) = J_1(\pi\alpha_{01}) [M \cos(\theta + \omega t - \delta_1) + N \cos(\theta - \omega t - \delta_2)] \quad (4)$$

This can be transformed to a simple sine function with a varying amplitude $A(t)$ and a varying phase $\varphi_{\text{pfr}}(t)$ as has been shown previously.¹⁹

$$p'(\theta, t) = A(t) \sin(\theta - \varphi_{\text{pfr}}(t)) \quad (5)$$

The combination of eq. (3), (4), and (5) together with the introduction of the $p_{\text{off}}(t)$ signal leads to the equation to calculate the $p'(t)$ signal of the 1T mode for any given position based on the results of the pressure field reconstruction algorithm.

$$p'(r, \theta, t) = A(t) \frac{J_1\left(\frac{\pi\alpha_{01}r}{R}\right)}{J_1(\pi\alpha_{01})} \sin(\theta - \varphi_{\text{pfr}}(t)) + p_{\text{off}}(t) \quad (6)$$

If the radius (r) is set to the radius of the cylinder (R) eq. (6) reduces to eq. (2) which is the equation for the wall pressure distribution in the pressure field reconstruction algorithm.

If the signals $A(t)$, $\varphi_{\text{pfr}}(t)$, and $p_{\text{off}}(t)$ of the pressure field reconstruction algorithm are used as input for eq. (6) it can be used to calculate the $p'(t)$ of the 1T mode at any given position within the measurement plane of the HF measurement ring ($r \leq R$, $\theta \in [0^\circ, 360^\circ)$).

3.3 Phase Analysis Methodology

The $I'(t)$ signals are filtered with exactly the same filter settings which were used for the filtering of the raw $p'_{\text{pdy}}(t)$ signals of the dynamic pressure sensors in the pressure field reconstruction procedure. This way the same frequency band is extracted out of the $I'(t)$ signals which was extracted out of the raw $p'_{\text{pdy}}(t)$ signals. The $p'(t)$ and $I'(t)$ signals now can be compared directly in order to calculate the phase shift signal $\varphi(t)$.

A first comparison of the two signals shows that the phase relation between them is not constant but continuously varying. For this reason the procedure to calculate the φ must be able to handle a varying φ between the analysed signals. Different approaches have been investigated in their ability to calculate the $\varphi(t)$ signal between the $p'(t)$ and $I'(t)$ signals from the BKD test runs. A general assumption which is common for all approaches is that both signals oscillate with the same frequency and can therefore be described by

$$p'(t) = \sin(\omega t - \varphi_p(t)) \quad (7)$$

$$I'(t) = \sin(\omega t - \varphi_I(t)) \quad (8)$$

It will be later shown that this assumption is not perfectly correct as the oscillation frequencies of $p'(t)$ and $I'(t)$ are not identical. The approach to calculate the $\varphi(t)$ signal is still valid as a frequency difference can also be represented by a linearly increasing or decreasing $\varphi(t)$.

In order to be able to capture a varying φ between both signals common to all investigated approaches is the division of both signals into blocks. In each block the φ is assumed to be constant. For each block the φ between both signals is calculated in order to compute a varying $\varphi(t)$ signal. The length of the blocks must be adjusted according to the rate of change of the φ . If the φ varies slowly the block length can be large in order to reduce the number of blocks and to decrease the computation time. Another advantage is that more data is available per block which facilitates the calculation of the φ . If the φ varies quickly compared to the oscillation frequency of the input signals, the block length must be small. This can be problematic if the block length becomes smaller than the period of one oscillation. Short blocks hinder the calculation of the φ for some approaches. In the case of the BKD data it was observed that the φ shows quick variations which makes it necessary to use a small block size of less than a period of the oscillation.

Next to the division of the signals into blocks, another step which is common to all investigated procedures is the normalisation of the input signals in order to facilitate the computation of the φ . Due to the band pass filtering both input signals are nearly mono frequent. This is a requirement for the whole methodology as the oscillation frequency of both signals is assumed to be equal and constant. This nearly mono frequent character of the signals enables an easy way to calculate the amplitude (envelope) signal by determining the maxima and minima of the signal. The input signal is then divided by the amplitude signal in order to obtain a signal with a constant amplitude of 1.

Due to the small block size required for the BKD data the cross correlation method which has been used previously to calculate the $\varphi(t)$ signal for data of the CRC research combustor¹⁶ was not applicable anymore as it caused large inaccuracies. For the same reason the determination of the φ by the measurement of the position of the zero crossing which creates very accurate results is not applicable. Therefore a phase fitting procedure has been used which worked well with small block sizes and showed good accuracy. As the phase of both signals and therefore also the phase shift φ is assumed to be constant in each block the normalised $p'(t)$ and $I'(t)$ inside the block are represented by

$$p'(t) = \sin(\omega t - \varphi_p) \quad (9)$$

$$I'(t) = \sin(\omega t - \varphi_I) \quad (10)$$

A sine function with one parameter (φ_{fit}) is fitted to both signals inside the block using a least-squares fitting procedure in order to obtain the values of φ_p and φ_I .

$$y(t) = \sin(\omega t - \varphi_{\text{fit}}) \quad (11)$$

These values are then used to calculate the the phase shift

$$\varphi = \varphi_p - \varphi_I \quad (12)$$

The $\varphi(t)$ signal with the sampling frequency of the $p'(t)$ and $I'(t)$ signals is then obtained using a cubic spline interpolation with the φ values of the blocks as input data. An exemplary result of this procedure to calculate the $\varphi(t)$ signal is shown in Figure 3. The plot shows the normalised input signals $p'(t)$ and $I'(t)$ together with the φ values of the blocks and the interpolated $\varphi(t)$ signal.

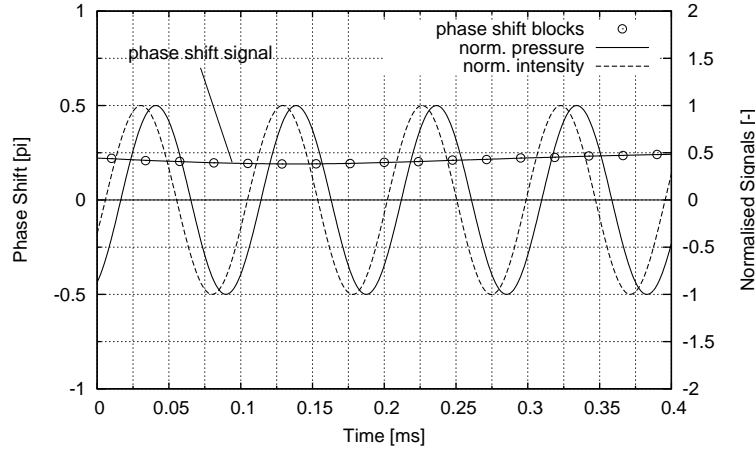


Figure 3: Exemplary result of the phase fitting procedure

3.4 Validation of Methodology

The methodology to calculate the $\varphi(t)$ signal presented here is a chain of different sub procedures. It consists of a number of sub steps to get from the raw data of the $p'_{\text{pdyn}}(t)$ signals and the $I'(t)$ signals to the final result of the $\varphi(t)$ signal. Therefore each sub step of the methodology has been tested and validated before the whole procedure has been applied to the BKD test data.

The pressure field reconstruction algorithm has been used several times for data from the CRC research combustor¹⁹ and the BKD.^{12,21} It is therefore seen as tested and validated at this point. In the work presented here it is tested together with the procedure from section 3.2 as a single module in order to validate eq. (6). The second sub procedure which requires testing and validation is the procedure to calculate the $\varphi(t)$ signal described in section 3.3.

In order to test the pressure field reconstruction together with the methodology from section 3.2 a 1T pressure field has been simulated using eq. (3). This equation has been used to calculate the signals $p'_{\text{pdyn}}(t)$ of the 8 dynamic pressure sensors. Furthermore this equation has been used to calculate the $p'(t)$ signal at a selected test position. Here the position of injector 10 has been chosen for this test position. The simulated sensor signals $p'_{\text{pdyn}}(t)$ have then been used as input for the pressure field reconstruction algorithm and the signals $A(t)$, $\varphi_{\text{pfr}}(t)$, and $p_{\text{off}}(t)$ were obtained. These signals were then used as input for eq. (6) to calculate the $p'(t)$ signal at the test position. This signal then was compared with the signal at the test position which was calculated using eq. (3) together with the simulated $p'_{\text{pdyn}}(t)$ signals. The result is shown in Figure 4 on the left side. As there is no difference visible between the simulated $p'(t)$ signal and the signal obtained with eq. (6) it is shown that the methodology reconstructs the $p'(t)$ signal at the test position with good accuracy.

The phase shift calculation procedure from section 3.3 is validated by simulating two signals $y_1(t)$ and $y_2(t)$ with a known $\varphi(t)$ signal and test the ability of the procedure to reconstruct this $\varphi(t)$ signal.

$$y_1(t) = A_1(t) \sin(\omega t) \quad (13)$$

$$y_2(t) = A_2(t) \sin(\omega t - \varphi(t)) \quad (14)$$

The amplitude signals $A_1(t)$ and $A_2(t)$ as well as the phase shift signal $\varphi(t)$ were simulated using a random number generator. The signals $y_1(t)$ and $y_2(t)$ were then used as input for the phase shift calculation procedure. As a result of this procedure the phase shift signal $\varphi(t)$ is obtained which is then compared with the simulated signal used in eq. (14). The result is shown in Figure 4 on the right side. As there is no difference visible between the simulated and the reconstructed $\varphi(t)$ signal it is shown that the methodology described in section 3.3 is able to reconstruct the $\varphi(t)$ signal with good accuracy.

4. Application to Test Data

The presented analysis methodology has been applied to two selected load points of a single test run of the BKD test series. These load points were selected as they incorporate one stable and one unstable load point. Figure 5 shows the test sequence of the selected test run with the signals of the combustion chamber pressure $p_{\text{cc}}(t)$ and mixture ratio

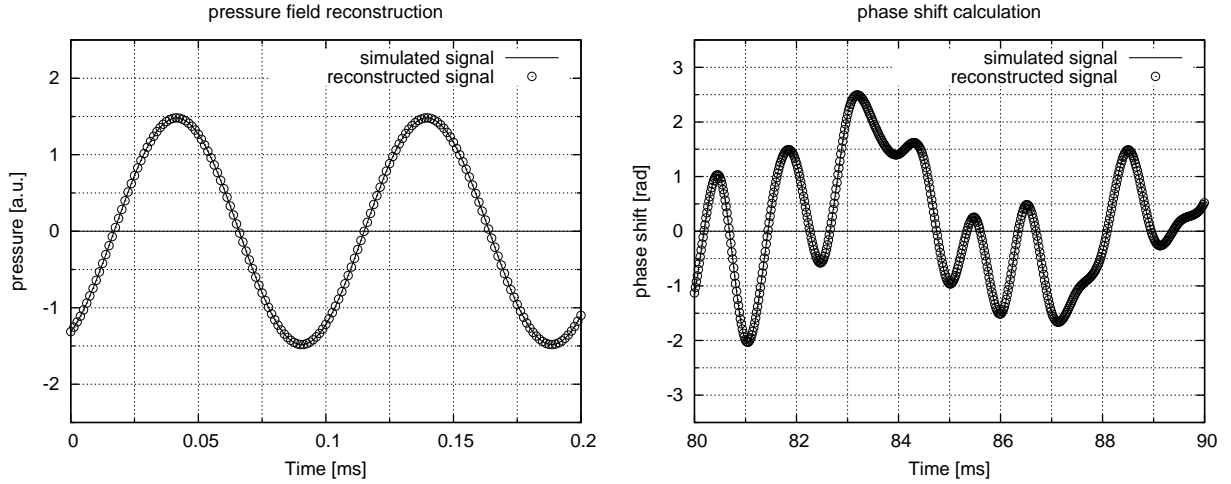


Figure 4: Validation of methodology: Signal at the test position calculated using the pressure field reconstruction (left). Reconstruction of a simulated phase shift signal (right).

ROF(t) together with one $p'_{\text{pdyn}}(t)$ signal of the dynamic pressure sensors in the HF measurement ring. The $p'_{\text{pdyn}}(t)$ signal shows increased oscillation amplitudes for the load point $p_{\text{cc}} = 80$ bar, ROF = 6. This is an instability of the 1T mode as has been shown in previous work.^{12,21} For the phase shift analysis this unstable load point (LP3) together with a stable load point (LP7, $p_{\text{cc}} = 60$ bar, ROF = 4) were selected. The corresponding analysis windows with a length of one second are marked in Figure 5 with gray areas.

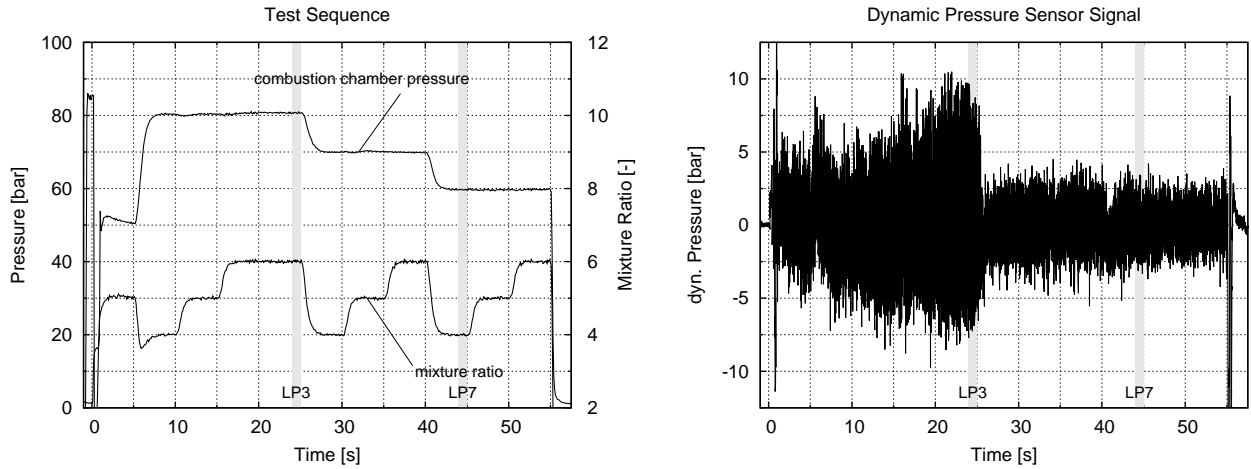


Figure 5: Test sequence of the selected test run with definition of analysis windows

For each analysis window 8 $p'_{\text{pdyn}}(t)$ and 3 $I'(t)$ signals are available. For the selected analysis windows the $\varphi(t)$ signal was calculated for the 3 injector positions observed by the fibre optical probes. Therefore a total number of 6 $\varphi(t)$ signals have been calculated, 3 for LP3 and 3 for LP7.

The band pass filter for the pressure field reconstruction algorithm is centered to the 1T frequency of the corresponding load point. For LP3 this is $f_{\text{LP3}} = 10239$ Hz and for LP7 $f_{\text{LP7}} = 10605$ Hz. The pass band width was set to 2800 Hz. In order to better resolve the rotational character of the 1T mode the signals are upsampled to a sampling frequency of 800 kHz.^{12,19,21} Using the results of the pressure field reconstruction the $p'(t)$ signals of the 1T mode are calculated for the 3 injector positions using the coordinates shown in Table 1. The $I'(t)$ signals were filtered with the same settings as the $p'_{\text{pdyn}}(t)$ signals. The $\varphi(t)$ signal is calculated with a block length of 0.5 periods of the 1T frequency with an overlap of 0.25 periods.

Table 1: Injector coordinates

injector	10	13	19
r [mm]	31	31	31
θ [°]	225	270	0
probe	C	B	A

5. Results

Figure 6 shows an exemplary $\varphi(t)$ signal as result of the phase shift calculation. The example is taken from the analysis of the unstable load point LP3. The plot shows the normalised $p'(t)$ signal at the position of injector 10 together with the normalised $I'(t)$ signal of probe C and the calculated $\varphi(t)$ signal. Plotted is a length of 5 ms which is 0.5% of the full length of the analysis window. The $\varphi(t)$ signal has been limited to the interval $[-\pi, \pi]$. Figure 6 clearly shows that the $\varphi(t)$ signal is characterised by a fluctuating behaviour on the time scales of the 1T oscillation period which is the case for all 6 calculated $\varphi(t)$ signals. Therefore statistical or signal analysis approaches are required in order to analyse the $\varphi(t)$ signals.

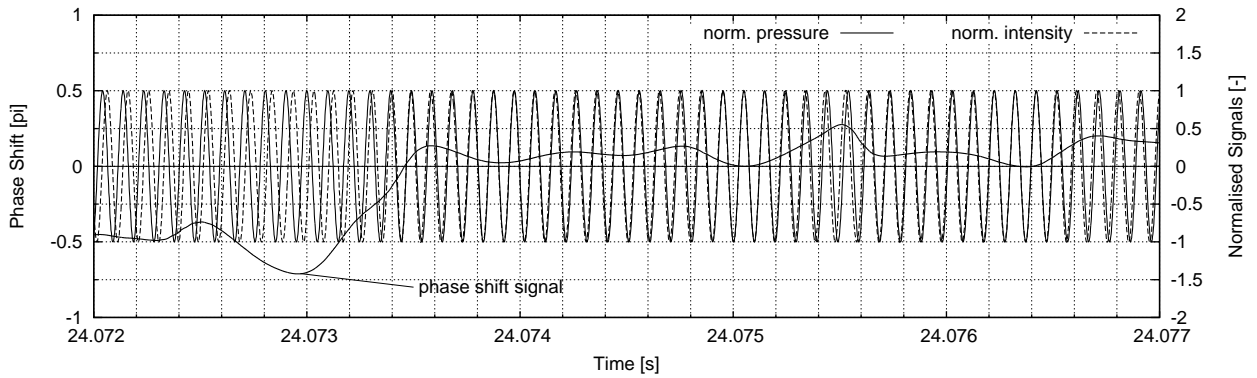


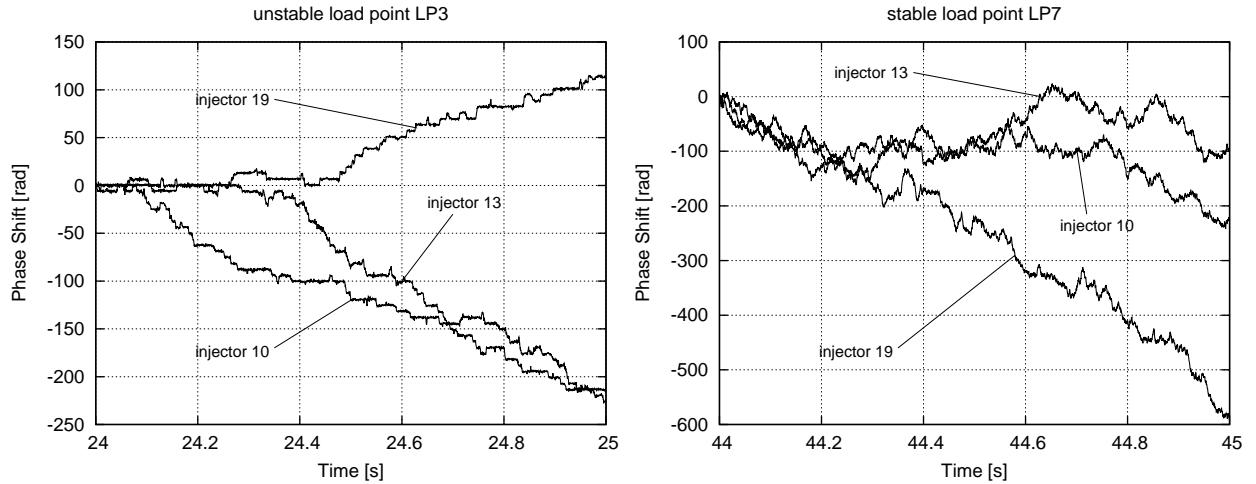
Figure 6: Exemplary result of the phase shift calculation

Generally there are two ways to represent the $\varphi(t)$ signal. First, the signal can be limited to the interval $[-\pi, \pi]$ as has been done for the plot in Figure 6. This representation is required in order to analyse the signal with regard to the Rayleigh criterion. Second, the values of $\varphi(t)$ can be represented without any limitation to a specific interval. This enables to analyse the signals in a different way: If both oscillations, $p'(t)$ and $I'(t)$ are characterised by slightly different oscillation frequencies this would cause a continuous increase or decrease of the $\varphi(t)$ signal.

Figure 7 shows the plot of all 6 calculated $\varphi(t)$ signals with no limitation to the interval $[-\pi, \pi]$. On the left side the signals of the 3 injectors are plotted for the unstable load point and on the right side for the stable load point. For both load points an average increase or decrease of the $\varphi(t)$ signals can be observed showing that the average oscillation frequencies of $p'(t)$ and $I'(t)$ are indeed not identical. Furthermore, for both load points the behaviour of all 3 signals is different. For LP3 the injectors 10 and 13 show a general decrease while injector 19 shows a general increase. For LP7 injector 19 shows a stronger general decrease than injector 10 and 13. An interesting aspect is that in both cases injector 19 shows a significantly different behaviour than the other two injectors. The plots show further a significant difference between the stable and unstable load point. For LP3 all $\varphi(t)$ signal are characterised by a more stepwise character. The signals stay in a specific region and then show a sudden jump. The signals of LP7 show a more continuous variation.

For both cases the increase or decrease of the $\varphi(t)$ signals on long time scales shows that the frequencies of $p'(t)$ and $I'(t)$ are not identical. The frequency of the $p'(t)$ signals for the 3 different positions on the other hand is always identical as these signals are created by the 1T mode which has at all positions the same frequency. The fact that the $\varphi(t)$ signals for the 3 different injectors show a different behaviour indicates that the 3 injectors behave differently. In other work by the authors²⁹ it was shown that the $I'(t)$ oscillations are created by the injectors. Furthermore indications were found that the oscillations created by the injectors are rather independent to the oscillations of the chamber pressure. The fact that all injectors create $I'(t)$ oscillations with slightly different behaviour supports these indications.

From the phase shift signals shown in Figure 7 an average frequency difference between the $p'(t)$ and $I'(t)$ signals can be estimated. These values are summarised in Table 2. The way the $\varphi(t)$ signal has been calculated a negative frequency difference Δf means that the average oscillation frequency of $I'(t)$ is lower than the average oscillation frequency of $p'(t)$ and the other way round. Figure 8 shows the power spectral density (PSD) of the 3 $I'(t)$ signals for

Figure 7: Plot of the 6 phase shift signals with no limitation to the interval $[-\pi, \pi]$

both load points. The peaks of the PSD signals are the injector resonance frequencies.²⁹ The pass band of the filter has been marked with a grey box. The PSD signals of the unstable load point show that the $I'(t)$ signal of injector 19 has a second, smaller peak at higher frequencies which the other signals do not have. This means, that the $I'(t)$ signal of injector 19 has components at higher frequencies with higher amplitudes compared to the $I'(t)$ signals of the other injectors which is in agreement with Table 2. The PSD signals of the stable load point show that also here the PSD of the $I'(t)$ signal of injector 19 shows a unique feature compared to the other signals. It shows a peak at approximately 9.5 kHz which does not exist in the PSD data of the other signals. This explains why the $\varphi(t)$ signal of injector 19 shows a much clearer trend for the stable load point than the $\varphi(t)$ signals of injector 10 and 13. The PSD data of the $I'(t)$ signals support the results of the phase shift analysis. Furthermore, the phase shift analysis has shown to be a very sensitive analysis methodology which is able to detect features in the signals which would not have been detected with a PSD analysis alone.

Table 2: Average frequency differences estimated from Figure 7

	LP3		LP7	
	$\Delta\omega$ [1/s]	Δf [Hz]	$\Delta\omega$ [1/s]	Δf [Hz]
injector 10	-220	-35	-220	-35
injector 13	-220	-35	-100	-16
injector 19	120	19	-600	-95

A second analysis which has been applied to the phase shift signals is to represent them in histogram plots. For this analysis the $\varphi(t)$ signals are restricted to the interval $[-\pi, \pi]$. This interval is divided into a number of sub intervals. For each sample of the $\varphi(t)$ signals it is decided to which interval it belongs to and the total number of samples of each interval is counted. This is an easy way to determine if there are any intervals in which the signal is to find with a higher probability and to identify if there is any structure in the signal.

Figure 9 shows the histograms of the 3 $\varphi(t)$ signals of the unstable load point LP3. The plots show very clearly that all 3 $\varphi(t)$ signals have a strong concentration of samples in the interval around $\varphi = 0$. This is generally in agreement with the expectations from the Rayleigh criterion. A φ around 0 causes an energy transfer from the heat release to the acoustic pressure oscillations. This explains the increased oscillation amplitudes for this load point. Also here injector 19 shows a slightly different behaviour compared to the injectors 10 and 13: The peak of the histogram is shifted slightly to positive values. The strong concentration of samples in a specific interval is in agreement with the results from Figure 7 where the $\varphi(t)$ signals of the unstable load point showed longer periods where they stayed in specific intervals.

Figure 10 shows the histograms of the 3 $\varphi(t)$ signals of the stable load point LP7. Here the plots show a completely different structure of the $\varphi(t)$ signals compared to the unstable load point. Also here a slight concentration of samples in specific intervals can be observed but this concentration is much less pronounced compared to the unstable case. Further this concentration is found in the interval between 0.2π and 0.6π which would result in lower ampli-

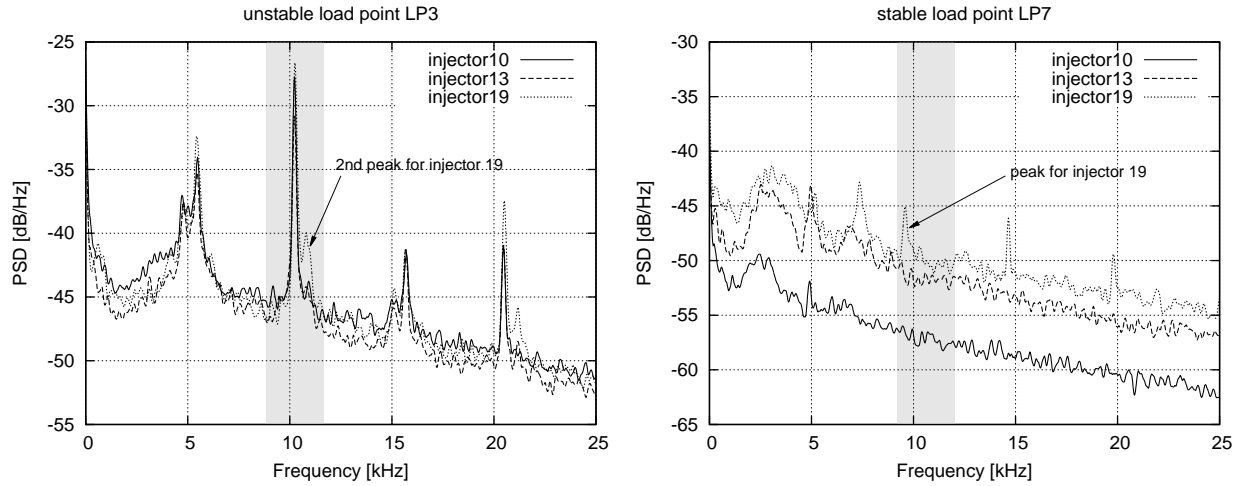


Figure 8: Power spectral density of the PM signals for the 2 selected load points with filter pass band

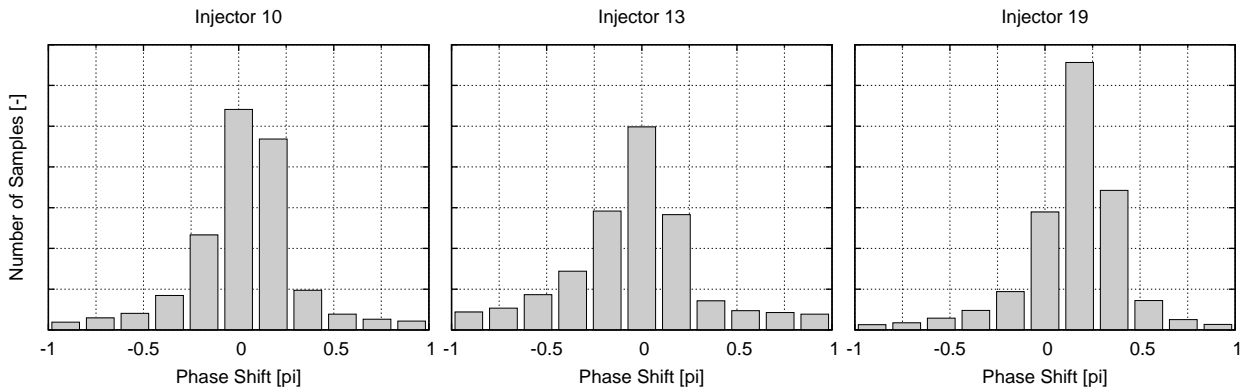


Figure 9: Histograms of the 3 phase shift signals of the unstable load point LP3

fication or even damping of the acoustic oscillations according to the Rayleigh criterion. The generally much less pronounced concentration of samples in specific intervals is in agreement with the results from Figure 7 which showed a much more continuous variation of the $\varphi(t)$ signals.

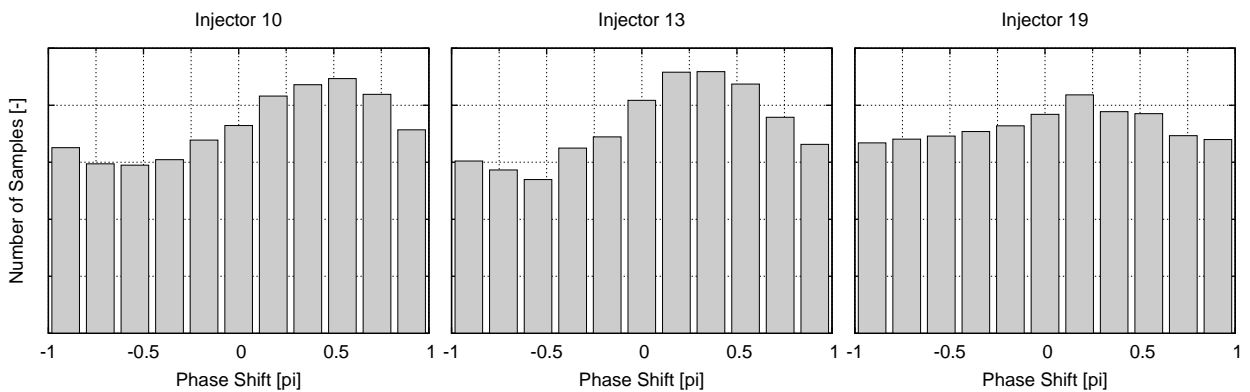


Figure 10: Histograms of the 3 phase shift signals of the stable load point LP7

The $\varphi(t)$ signals of the stable and unstable load point show significant differences. The signals of the unstable load point show a concentration of samples in a region which causes an amplification of the acoustic pressure oscillations according to the Rayleigh criterion. The signals of the stable load point show a much less pronounced concentration

of samples in specific intervals. This means that periods of damping and driving are more equally distributed for the stable load point while the unstable load point is characterised by longer periods of driving.

6. Summary and Conclusions

A phase shift analysis study has been performed with experimental data from a research combustor named BKD. This combustor shows self-excited combustion instabilities of the 1T mode for specific load points. The combustion chamber has been equipped with dynamic pressure sensors to measure the acoustic pressure oscillations as well as fibre optical probes to measure the OH* intensity oscillations as a measure for the heat release rate oscillations. The fibre optical probes were aligned to 3 selected injectors in order to measure the OH* intensity fluctuation generated by these injectors. The dynamic pressure sensor signals and the optical signals have been processed using a newly developed analysis methodology.

The dynamic pressure sensor signals are processed with a 1T mode pressure field reconstruction procedure. The results of this procedure are used to calculate the pressure oscillations of the 1T mode at the positions of the 3 selected injectors. The optical signals are band pass filtered to the frequency of the 1T mode pressure oscillations. As a result of this preparation for all 3 injector positions a pressure oscillation and an OH* intensity oscillation signal are available which are used as input for a phase shift analysis procedure. This procedure calculates a phase shift signal which describes the phase shift between the pressure and OH* intensity oscillation.

The analysis methodology has been applied to 2 selected load points (one stable and one unstable) of a single test run of the BKD test series. Generally the calculated phase shift signals show that the phase relation between the pressure and OH* intensity oscillation is not constant. The phase shift signals show fluctuations on the time scales of the oscillation frequency of the analysed signals. On long time scales on the other hand they show a trend which can be explained by different oscillation frequencies of the pressure and OH* intensity signals. It has been shown previously that the oscillation frequencies of pressure and OH* are not identical which is supported by the results of the phase shift analysis. Furthermore the analysis was able to detect differences in the dynamics of the observed injectors. Two injectors show a similar behaviour while the third one deviates from the others. The reason for this behaviour could not be identified so far but a power spectral density analysis of the OH* intensity signals supports the results of the phase shift analysis. The phase shift signals of the unstable load point show a concentration of samples around the value of zero which is in agreement with the Rayleigh criterion. The signals of the stable load point on the other hand show a much more equal distribution over the interval $[-\pi/\pi]$ meaning that periods with damping and driving are much more equally distributed for this load point.

The newly developed methodology has shown to be applicable to the experimental data of the BKD test series. It has shown to be able to discover new information about the dynamic processes of BKD. The procedure is a very sensitive analysis method which is able to detect aspects of the dynamic processes with a high level of detail. The complexity of the resulting phase shift signals hinder the analysis of these signals. Further analysis of the currently calculated 6 signals is therefore required. Up to now the methodology has only been applied to two load points of a single test run. The analysis needs to be extended to other load points and test runs of the BKD test series in order to form a statistical basis for the discovery of general trends which is not possible with the analysis of only two selected load points.

Acknowledgements

Research undertaken for this paper has been assisted with financial support from the DFG (German Research Foundation) in the framework of the SFB-TR 40. The Authors are grateful to the crew of the P8 test bench as well as Philipp Groß and Mike Ziemßen for their efforts in performing the test runs on which the results presented here are based. Furthermore the efforts of Joachim Sender concerning the design of the BKD combustor are gratefully acknowledged.

References

- [1] Ross, C. C. and Datner, P. P. Combustion Instability in Liquid-Propellant Rocket Motors—A Survey. In W. R. Hawthorne, J. Fabri, and D. B. Spalding, editors, *Selected Combustion Problems*, 352–380. Butterworths Scientific Publications, 1954. Advisory Group for Aeronautical Research and Development North Atlantic Treaty Organization.
- [2] Anderson, W. E., Ryan, H. M., and Santoro, R. J. Combustion instability phenomena of importance to liquid bi-propellant rocket engine. In 28th JANNAF Combustion Subcommittee Meeting. 1991.
- [3] Harrje, D. T. and Reardon, F. H. *Liquid Propellant Rocket Combustion Instability*. NASA Special Publication SP-194, NASA, 1972.
- [4] Yang, V. and Anderson, W. E., editors. *Liquid Rocket Engine Combustion Instability*, volume 169 of *Progress in Astronautics and Aeronautics*. American Institute of Aeronautics and Astronautics, Washington, DC, 1995.
- [5] Pieringer, J. and Sattelmayer, T. Simulation of Combustion Instabilities in Liquid Rocket Engines with Acoustic Perturbation Equations. *Journal of Propulsion and Power*, 25(5):1020–1031, 2009.
- [6] Schulze, M., Schmid, M., Morgenweck, D., Köglmeier, S., and Sattelmayer, T. A Conceptual Approach for the Prediction of Thermoacoustic Stability in Rocket Engines. In 49th AIAA/ASME/SAE/ASEE Joint Propulsion Conference. San Jose, CA, 2013. AIAA 2013-3779.
- [7] Rayleigh, J. W. S. The Explanation of Certain Acoustical Phenomena. *Nature*, 18(455):319–321, 1878.
- [8] Rayleigh, J. W. S. *The Theory of Sound*, volume 2. Dover Publications, New York, 2 edition, 1945.
- [9] Putnam, A. A. and Dennis, W. R. Burner oscillations of the gauze-tone type. *Journal of the Acoustical Society of America*, 26(5):716–725, September 1954.
- [10] Putnam, A. A. and Dennis, W. R. Organ-Pipe Oscillations in a Flame-Filled Tube. In Fourth Symposium (International) on Combustion, 566–575. The Standing Committee on Combustion Symposia, The Williams & Wilkins Company, Baltimore, 1953.
- [11] Sutton, G. P. and Biblarz, O. *Rocket Propulsion Elements*. John Wiley & Sons, New York, 7 edition, 2001.
- [12] Gröning, S., Oswald, M., and Sattelmayer, T. Selbst erregte tangentielle Moden in einer Raketenbrennkammer unter repräsentativen Bedingungen. In 61. Deutscher Luft- und Raumfahrtkongress. Deutsche Gesellschaft für Luft- und Raumfahrt - Lilienthal-Oberth e.V. (DGLR), Berlin, September 2012.
- [13] Richecoeur, F., Scoufflaire, P., Ducruix, S., and Candel, S. High-Frequency Transverse Acoustic Coupling in a Multiple-Injector Cryogenic Combustor. *Journal of Propulsion and Power*, 22(4):790–799, July-August 2006.
- [14] Knapp, B. and Oswald, M. High Speed Visualization of Flame Response in a LOX/H₂ Combustion Chamber During External Excitation. In 12th International Symposium on Flow Visualization. Göttingen, September 2006.
- [15] Oswald, M. and Knapp, B. Investigation of Combustion Chamber Acoustics and its Interaction with LOX/H₂ Spray Flames. In L. T. DeLuca, C. Bonnal, O. Haidn, and S. M. Frolov, editors, *Progress in Propulsion Physics*, volume 1 of *EUCASS proceedings series - Advances in Aerospace Sciences*, 205–224. 2009.
- [16] Sliphorst, M., Knapp, B., Groening, S., and Oswald, M. Combustion Instability-Coupling Mechanisms Between Liquid Oxygen/Methane Spray Flames and Acoustics. *Journal of Propulsion and Power*, 28(6):1339–1350, November-December 2012.
- [17] Hardi, J. S., Beinke, S. K., Oswald, M., and Dally, B. B. Coupling of Cryogenic Oxygen-Hydrogen Flames to Longitudinal and Transverse Acoustic Instabilities. *Journal of Propulsion and Power*, 30(4):991–1004, July-August 2014.
- [18] Quinlan, J. M. and Zinn, B. T. Transverse Combustion Instabilities: Modern Experimental Techniques and Analysis. In 50th AIAA/ASME/SAE/ASEE Joint Propulsion Conference. American Institute of Aeronautics and Astronautics, Cleveland, OH, July 2014.
- [19] Sliphorst, M., Gröning, S., and Oswald, M. Theoretical and Experimental Identification of Acoustic Spinning Mode in a Cylindrical Combustor. *Journal of Propulsion and Power*, 27(1):182–189, January-February 2011.

- [20] Suslov, D., Woschnak, A., Sender, J., and Oswald, M. Test Specimen Design and Measurement Technique for Investigation of Heat Transfer Processes in Cooling Channels of Rocket Engines under Real Thermal Conditions. In 39th AIAA/ASME/SAE/ASEE/JPC Conference and Exhibit. Huntsville, AL, 2003. AIAA 2003-4613.
- [21] Gröning, S., Suslov, D., Oswald, M., and Sattelmayer, T. Stability behaviour of a cylindrical rocket engine combustion chamber operated with liquid hydrogen and liquid oxygen. In 5th European Conference for Aeronautics and Space Sciences (EUCASS). Munich, July 2013.
- [22] Fröhlke, K., Haberzettl, A., Haidn, O. J., Heinrich, S., Sion, M., and Vuillermoz, P. First Hot Fire Test Campaign at the French/German Research Facility P8. In 33rd AIAA/ASME/SAE/ASEE Joint Propulsion Conference. Seattle, WA, 1997.
- [23] Koschel, W. and Haidn, O. J. P8 - The New French/German Test Facility For H₂/O₂ High Pressure Rocket Engine Combustion Research. *International Journal of Hydrogen Energy*, 23(8):683–694, August 1998.
- [24] Haberzettl, A. European Research And Technology Test Bench P8 For High Pressure Liquid Rocket Propellants. In 36th AIAA/ASME/ASEE Joint Propulsion Conference and Exhibit. Huntsville, Alabama, July 2000. AIAA 2000-3307.
- [25] Fiala, T. and Sattelmayer, T. Heat Release and OH*-Radiation in Laminar Non-Premixed Hydrogen-Oxygen Flames. In 51st AIAA Aerospace Sciences Meeting including the New Horizons Forum and Aerospace Exposition. Grapevine, Texas, 2013.
- [26] Fiala, T. and Sattelmayer, T. On the Use of OH* Radiation as a Marker for the Heat Release Rate in High-Pressure Hydrogen-Oxygen Liquid Rocket Combustion. In 49th AIAA/ASME/SAE/ASEE Joint Propulsion Conference and Exhibit. San Jose, CA, 2013. AIAA 2013-3780.
- [27] Spicher, U. and Velji, A. Measurements of Spatial Flame Propagation and Flow Velocities in a Spark Ignition Engine. In Twentieth Symposium (International) on Combustion, volume 20, 19–27. 1985.
- [28] Pöschl, M. Einfluss von Temperaturinhomogenitäten auf den Reaktionsablauf bei der klopfenden Verbrennung. Ph.D. thesis, Technische Universität München, München, 2006.
- [29] Gröning, S., Hardi, J. S., Suslov, D., and Oswald, M. Injector-driven combustion instabilities in a hydrogen/oxygen rocket combustor. *Journal of Propulsion and Power*, 2015. Submitted for publication to the Journal of Propulsion and Power.
- [30] Knapp, B., Farago, Z., and Oswald, M. Interaction of LOX/GH₂ Spray-Combustion with Acoustics. In 45th AIAA Aerospace Sciences Meeting and Exhibit. American Institute of Aeronautics and Astronautics, Reno, Nevada, January 2007. AIAA 2007-0572.
- [31] Stearns, S. D. Digital Signal Analysis. Hayden Book Company, Rochelle Park, 1975.
- [32] Zucrow, M. J. and Hoffmann, J. D. Gas Dynamics, volume II. Robert E. Krieger Publishing Company, Malabar, 2nd edition, 1985.